Accepted Manuscript published as JOE-19-0279.R1. Accepted for publication: 19-Aug-2019

Thermoneutrality improves skeletal impairment in adult Prader-Willi syndrome mice

Thomas M Braxton[1], Dionne EA Sarpong[1], Janine L Dovey[1], Anne Guillou[2], Bronwen AJ Evans[3], Juan M Castellano[4], Bethany E Keenan[5], Saja Baraghithy[6], Sam L Evans[5], Manuel Tena-Sempere[4,7], Patrice Mollard[2], Joseph Tam[6] and Timothy Wells[1*]

[1]School of Biosciences, Cardiff University, Museum Avenue, Cardiff, CF10 3AX, UK
[2]IGF, CNRS, INSERM, University of Montpellier, Montpellier, France
[3]School of Medicine, Cardiff University, Cardiff CF14 4XN, UK
[4]Physiology Section, Faculty of Medicine, University of Cordoba, and Instituto Maimonides de Investigacion Biomedica de Cordoba (IMBIC), 14004 Cordoba, Spain
[5]School of Engineering, Cardiff University, The Parade, Cardiff, CF24 3AA, UK
[6]Obesity and Metabolism Laboratory, Institute for Drug Research, School of Pharmacy, Faculty of Medicine, The Hebrew University of Jerusalem 9112001, Israel
[7]CIBER Fisiopatologia de la Obesidad y Nutrición (CIBEROBN), Instituto de Salud Carlos III, 14004 Cordoba, Spain

Running head: Skeletal Phenotype in PWS-IC*del* Mice

Word Count: 4986 (including the Abstract)

***Author for correspondence:**

Dr Timothy Wells
School of Biosciences,
Cardiff University,
Cardiff. CF10 3US, UK
Tel: (+44) 2920 874977
Fax: (+44) 2920 876328
E-mail: wellst@cardiff.ac.uk

Abstract

Human Prader-Willi syndrome (PWS) is characterised by impairments of multiple systems including the growth hormone (GH) axis and skeletal growth. To address our lack of knowledge of the influence of PWS on skeletal integrity in mice, we have characterised the endocrine and skeletal phenotype of the PWS-IC^{del} mouse model for "full" PWS and determined the impact of thermoneutrality.

Tibial length, epiphyseal plate width and marrow adiposity were reduced by 6%, 18% and 79% in male PWS-IC^{del} mice, with osteoclast density being unaffected. Similar reductions in femoral length accompanied a 32% reduction in mid-diaphyseal cortical diameter. Distal femoral Tb.N was reduced by 62%, with individual trabeculae being less plate-like and the lattice being more fragmented (Tb.Pf increased by 63%). Cortical strength (Ultimate moment) was reduced by 26% as a result of reductions in calcified tissue strength and the geometric contribution. GH and prolactin contents in PWS-IC^{del} pituitaries were reduced in proportion to their smaller pituitary size, with circulating IGF-1 concentration reduced by 37-47%. Conversely, while pituitary LH content was halved, circulating gonadotropin concentrations were unaffected. Although longitudinal growth, marrow adiposity and femoral geometry were unaffected by thermoneutrality, strengthened calcified tissue reversed weakened cortex of PWS-IC^{del} femora.

While underactivity of the GH-axis may be due to loss of *Snord116* expression and impaired limb bone geometry and strength due to loss of *Magel2* expression, comprehensive analysis of skeletal integrity in the single gene deletion models is required. Our data imply that thermoneutrality may ameliorate the elevated fracture risk associated with PWS.

Accepted Manuscript published as JOE-19-0279.R1. Accepted for publication: 19-Aug-2019

Introduction

Prader-Willi syndrome (PWS) is a neurodevelopmental disorder arising from the loss of expression of one or more genes from the paternal allele of the PWS locus (Butler *et al*, 2016). The PWS phenotype is complex, characterised by neonatal hypotonia and an initial failure to thrive (Miller *et al*, 2011), the subsequent development of hyperphagia (Miller *et al*, 2011), hyperghrelinaemia (Cummings *et al*, 2002), and growth hormone (GH) deficiency (Grosso *et al*, 1998), resulting in severe truncal obesity and growth retardation (Kahn *et al*, 2018).

By manipulating the murine PWS locus on chromosome 7, several mouse models for this condition have linked the contribution of individual PWS genes to specific phenotypic characteristics. For example, while loss of the *MAGE*-family gene, *Necdin* has no effect on growth or adiposity (Cattanach *et al*, 1992, Muscatelli *et al*, 2000) *Necdin*-null mice display enhanced differentiation and/or proliferation of astrocytes (Fujimoto et al, 2016), neocortical neural precursor cells (Minamide et al, 2014), hematopoietic stem cells (Asai et al, 2012) and pre-adipocytes (Fujiwara *et al*, 2012). Similarly, although deletion of another *MAGE*-family gene, *Magel2*, fails to induce hyperphagia with standard diets (Bischof *et al*, 2007), *Magel2*-null mice display impaired GH axis function (Tennese & Wevrick, 2011) and leptin sensitivity (Pravdivyi *et al*, 2015), accompanied by a doubling of fat mass (Bischof *et al*, 2007). In contrast, loss of the small nucleolar (sno)RNA, *Snord116*, results in mild hyperphagia and impaired meal-termination, but accompanied by intra-abdominal leanness (Ding *et al*, 2008).

Such studies have revealed features of PWS not commonly reported in humans. For example, our study of metabolic homeostasis in the PWS-IC^{del} mouse, in which paternal inheritance of an imprinting centre (IC) deletion results in a complete lack of gene expression from the entire PWS interval (Chamberlain *et al*, 2004), revealed overactive brown fat and excess heat production (Golding *et al*, 2017). Unlike humans with PWS (Kahn *et al*, 2018), PWS-IC^{del} mice display profound abdominal leanness, probably resulting from a compromised capacity of PWS adipocytes to import lipid (Golding *et al*, 2017), a phenomenon reported in isolated human PWS adipocytes (Cadoudal *et al*, 2014).

Disruption of adipocyte function has extra-metabolic consequences. For example, there is a bi-directional relationship between fat and bone (Leiben *et al*, 2009), with bone marrow adipocytes and the bone-forming osteoblasts arising from the same mesenchymal stem cells (MSCs) (Beresford *et al*, 1992, Di Iorgi *et al*, 2008) and osteogenesis being influenced by leptin (Thomas *et al*, 1999, Hamrick *et al*, 2005, Evans *et al*, 2011). Although several studies have examined the effects of the loss of specific PWS interval regions/genes on bone (Khor *et al*, 2016, Kamaludin *et al*, 2016, Baraghithy *et al*, 2019), a study of the impact of losing all of the genes in the PWS locus is lacking. We have therefore conducted a study of the growth, morphology, microarchitecture and biomechanical properties of the appendicular bones of PWS-IC^{del} mice and characterised the underlying endocrine phenotype. In addition, since we have recently shown that maintaining PWS-IC^{del} mice at thermoneutrality may reduce proportionate hyperphagia (Golding *et al*, 2017), we quantified the effect of this manipulation on bone morphology and strength.

 Accepted Manuscript published as JOE-19-0279.R1. Accepted for publication: 19-Aug-2019

Materials and Methods

Animals

The mice used in this study were bred under the authority of the Animals (scientific procedures) Act 1986 (UK), with subsequent procedures conforming with the ARRIVE guidelines and specifically approved by the Cardiff University Animal Welfare Ethical Review Body (AWERB).

PWS-IC$^{m+/p-}$ (referred to throughout as PWS-IC^{del}) and wild-type (WT) littermates were generated by crossing IC^{del}-positive males with WT females. Given that PWS-IC^{del} animals on a pure C57BL/6J background suffer severe postnatal lethality (Yang et al, 1998), we crossed IC^{del} positive males with CD1 females and selectively culled WT littermates (identified on the basis of their increased size 48 hours after birth) leaving only 1 or 2 WT pups per litter (Chamberlain *et al*, 2004). Animals were weaned at approximately 4 weeks of age and housed in single-sex groups with WT littermates (2-5 animals per cage).

All animals were maintained on a 12hr light/dark cycle (lights on 07:00h) at 20-22°C (unless otherwise stated), with *ad libitum* access to water and standard laboratory chow (Rat and Mouse No. 3 Breeding Diet, Special Diet Services Ltd., Witham, Essex, UK, containing 4.2% crude fat; 22.4% crude protein; 4.2% crude fibre; 7.6% crude ash (see Tilston et al, 2019 for full dietary composition).

Study 1. Tibial growth and marrow adiposity in PWS-IC^{del} mice

After an overnight fast (with water available *ad libitum*), 18-month old male PWS-IC^{del} and WT littermates were killed by cervical dislocation. Left tibiae were excised, the length determined with a hand-held micrometer and fixed in buffered formal saline for 48hrs at 4°C before being decalcified in 0.5M EDTA (pH 7.6). Tibiae were stored in 70% ethanol at 4°C prior to quantifying epiphyseal plate width (EPW), marrow adiposity and osteoclast number (see below).

Study 2. Femoral phenotype in PWS-IC^{del} mice

Left femora were excised from the mice in study 1, soft tissue removed and length measured with a hand-held micrometer. Femora were wrapped in saline-soaked gauze, snap frozen and stored at -80°C for subsequent μ-CT and biomechanical analysis (see below).

Study 3. Endocrine status in PWS-IC^{del} mice

Male and female PWS-IC^{del} and their 6-15-month old WT littermates were anaesthetised with isoflurane and killed by decapitation. Pituitaries were dissected, weighed, snap frozen and stored at -80°C for subsequent quantification of growth hormone (GH), prolactin (PRL) and luteinising hormone (LH) content (see below).

Male and female PWS-IC^{del} and their 5-9-month old WT littermates were anaesthetised with isoflurane and killed by decapitation. Pituitaries were dissected and weighed and trunk blood collected into EDTA-coated tubes, vortexed and centrifuged. Aliquots of separated plasma were snap frozen and stored at -80°C for subsequent quantification of circulating insulin-like growth factor-1 (IGF-1), LH and follicle stimulating hormone (FSH) (see below).

Study 4. The effect of thermoneutrality on skeletal parameters in PWS-IC^{del} mice

Accepted Manuscript published as JOE-19-0279.R1. Accepted for publication: 19-Aug-2019

Male and female PWS-IC^{del} and their 6-15-month old WT littermates were group-housed in standard mouse cages (2-3 mice /cage) at 20-22°C or at thermoneutrality (30°C) (Golding *et al*, 2017). After 9 weeks, mice were anaesthetised with isoflurane and killed by decapitation. Tibiae and femora were excised and processed as above (studies 1 & 2) for subsequent quantification of growth, adiposity, geometry and strength.

Quantification of tibial epiphyseal plate width and marrow adiposity

Tibial EPWs and marrow adiposity were measured as previously described (Gevers *et al*, 2002; Thompson *et al*, 2004, Navein *et al*, 2016, Hopkins *et al*, 2017). In brief, three 7µm anterior-posterior longitudinal tibial sections were stained with Masson's Trichrome and visualised under light microscopy. Total plate width was measured in triplicate on digitally captured images of each section using the interactive feature tool of Leica QWin (V3.2). Marrow adiposity was quantified on digital images of mid-diaphyseal marrow and photomicrographs analysed with National Institutes of Health (NIH) Image J, to quantify %-adiposity, and the number and size of marrow adipocytes.

Quantification of tibial osteoclasts

To identify osteoclasts, consecutive paraffin sections were de-parraffinised, stained for tartrate-resistant acid phosphatase (TRAP; Sigma-Aldrich), and counterstained with Mayer's haematoxylin. Histomorphometric analysis was performed on digital photomicrographs using IMAGE-PRO PLUS V.6 (Media Cybernetics, Silver Spring, MD) to determine the number of TRAP$^+$ osteoclasts per bone surface (N.Oc/BS).

Quantification of femoral trabecular architecture

The trabecular microarchitecture of the distal femora was assessed using a high-resolution µ-CT system (Bruker Skyscan 1272, Kontich, Belgium) as previously described in rats (Evans *et al*, 2011) and mice (Navein *et al*, 2016). Femora were thawed, mounted on the sample presentation stage and orientated by taking a series of single images. Scanning was conducted at 70kV and 142µA, using a resolution of 9.04µm, 990 millisecond exposures, a rotation step of 0.60° and a 0.5mm aluminium filter. Analysis was performed according to the ASBMR guidelines (Bouxsein *et al*, 2010). In brief, a 1mm^3 ROI of secondary spongiosa 0.5mm above the centre of the distal epiphyseal plate was analyzed using the CT image analysis software (CT-An; https://www.bruker.com/products/microtomography/micro-ct-software/3dsuite.html). Trabecular bone was separated from cortical bone within the area of interest by using the freehand drawing tool in CT-An. After scanning, femora were re-wrapped in saline-soaked gauze and re-frozen and for strength testing.

Biomechanical testing

Mechanical strength of the femoral cortex was quantified by three-point bending as previously described (Stevenson *et al*, 2009, Navein *et al*, 2016), with the lower rollers set at 6.42 and 4.04 mm apart for WT and PWS-IC^{del} femora respectively and the central roller positioned equidistant from the lower rollers over the thinnest part of the mid-diaphyseal region, to give an approximately posterior load direction. Femora were loaded at a crosshead speed of 2mm/min until failure, with load and displacement data recorded by a Zwick Z050 tensile testing machine fitted with a 1kN load cell (Zwick Testing Machines Ltd., Leominster, United Kingdom). Ultimate tensile stress was calculated using failure load, morphometric measurements of cortical wall thicknesses and diameter (taken from cross-sectional µ-CT images corresponding to the fracture site as determined by measuring the distance from the end of the femur to the fracture point using a hand-held micrometer) and simple beam theory.

 Accepted Manuscript published as JOE-19-0279.R1. Accepted for publication: 19-Aug-2019

Hormone Quantification

Pituitaries were homogenized in 0.5ml lysis buffer (TRIS 0.1M pH 7.4, NaCl 0.15M, EGTA 1mM, EDTA 1mM, Triton 1%, Protease inhibitor cocktail (Sigma-Aldrich, P8340) and Phosphatase inhibitor cocktail 3 (Sigma- Aldrich, P0044)), maintained on ice for 30 mins and centrifuged for 10 mins at 13000g. Protein concentration was measured in a 1:100 dilution of 4μl of the supernatant with the QuantiPro BCA assay kit (Sigma Aldrich, QPBCA-1KT) using protein standards (Sigma-Aldrich, P0914). Samples were diluted in PBS to normalize protein concentration. GH, LH and PRL levels were measured using sandwich ELISAs (Steyn *et al*, 2011; Steyn *et al*, 2013, Guillou *et al*, 2015).

Plasma IGF-1 concentrations were determined in duplicate using a rat/mouse total IGF-1 immunoenzymometric assay (OCTEIA® Immunodiagnostic Systems Ltd., #AC-18F1) according to the manufacturer's instructions, with samples pre-treated to avoid binding protein interference. LH and FSH levels were measured in plasma samples using radioimmunoassay reagents provided by the National Institutes of Health (Dr. A. F. Parlow, Torrance, CA, USA). Rat LH-I-10 and FSH-I-9 were labeled with ^{125}I by the chloramine-T method, and LH and FSH concentrations expressed using reference preparations LH-RP-3 and FSH-RP-2 as standards. Intra- and inter-assay coefficients of variation were <8% and <10% for LH and <6% and <9% for FSH, respectively. Assay sensitivities were 5 pg/tube for LH and 20 pg/tube for FSH.

Statistical analyses

Results are expressed as mean ± SEM, and compared by unpaired Student's t-test or 1-way ANOVA and Bonferroni's selected pairs *post hoc* test (using GraphPad Prism, GraphPad Software Inc., San Diego. CA., USA), as indicated in the figure legends, with $P < 0.05$ considered significantly different.

Results

Study 1. Tibial growth and marrow adiposity in PWS-IC^{del} mice

Tibial length and EPW were reduced in PWS-IC^{del} males by 6% (P<0.001; Fig 1A) and 18% (P<0.01; Fig 1B) respectively. A profound (79%) reduction in tibial marrow adiposity (P<0.05; Fig 1C and inset pictures a & b) was due to a combination of a 53% reduction in marrow adipocyte number (P<0.05; Fig 1D) and a 48% reduction in mean adipocyte size (P<0.05; Fig 1E). Adipocyte size profiling (Fig 1F) revealed a loss of larger adipocytes, especially those >825µm^2 (P<0.05).

Analysis of TRAP$^+$-stained sections revealed a 62% reduction in tibial osteoclast number (P<0.05; data not shown), but when corrected for the 65% reduction in tibial trabecular surface (P<0.05; data not shown), the osteoclast density was unaffected (P=0.403; Fig 1G).

Study 2. Femoral phenotype in PWS-IC^{del} mice

A 4% reduction in femoral length in PWS-IC^{del} mice (P<0.05; Fig 2A) was accompanied by a 32% reduction in cortical (anterior-posterior) diameter (P<0.05; Fig 2B) with mean cortical wall thickness in PWS-IC^{del} mice being 73% of that in WT littermates (P=0.055; Fig 2C). µCT analysis revealed that trabecular number (Tb.N) in the distal femora of PWS-IC^{del} mice was reduced by 62% (P<0.01; Fig 2D). Although the overall trabecular thickness (Tb.Th) was unaffected (P=0.110; Fig 2E), the cross-sectional shape became more cylindrical (less plate-like) in PWS-IC^{del} mice (structural modal index (SMI) increased by 25%; P<0.05; Fig 2F). Trabecular surface was reduced in PWS-IC^{del} femora by 72% (P=0.0006; data not shown), but when corrected for the 77% reduction in trabecular volume (P=0.0009; data not shown), relative trabecular surface (BS/BV) was

Accepted Manuscript published as JOE-19-0279.R1. Accepted for publication: 19-Aug-2019

increased by 29% (*P*<0.01; Fig 2G). These changes were accompanied by an 18% increase in trabecular separation (Tb.Sp; *P*<0.01; Fig 2H) and a marked fragmentation of the trabecular lattice (63% increase in Pattern factor (Tb.Pf; *P*<0.05; Fig 2I). Although mean degree of anisotropy in PWS-IC^{del} mice was 125% of that in WT littermates, this index of trabecular orientation was not significantly different (*P*=0.098; data not shown).

Biomechanical strength of PWS-IC^{del} femoral cortex was reduced by 26% (ultimate moment; *P*<0.05; Fig 3A). This was due to an 80% decrease in the geometric contribution to strength (second moment of area; P<0.05; Fig 3C), the strength of the calcified tissue (ultimate tensile stress; UTS) being increased by 65% (*P*<0.05; Fig 3B).

Study 3. Endocrine status in PWS-IC^{del} mice

To investigate whether skeletal impairment might be due to endocrine dysfunction, we quantified pituitary and circulating hormone concentrations. Although not sexually dimorphic in either WT or PWS-IC^{del} mice, pituitary weight was reduced in both male and female PWS-IC^{del} mice by 35% and 43% respectively (*P*<0.01 and *P*<0.001; Fig 4A). Similarly, pituitary GH content was reduced by 42% and 56% in male and female PWS-IC^{del} mice (P<0.05; Fig 4B), in proportion to protein content (data not shown). While average pituitary PRL content in male PWS-IC^{del} mice was only 45% of that in WT males, this was not significantly different (*P*>0.05). In contrast, female PWS-IC^{del} mice showed a 41% reduction in PRL content (*P*<0.05; Fig 4C); the marked sexual dimorphism seen in WT mice (*P*<0.0001) being retained in PWS-IC^{del} littermates (*P*<0.01; Fig 4C). This sexual dimorphism (*P*<0.0001), but not PRL deficiency, was retained when PRL contents were corrected for protein content (data not shown). Male PWS-IC^{del} mice showed a marked (58%) reduction in pituitary LH content (P<0.0001; Fig 4D), but while mean LH content in female PWS-IC^{del} mice was only 54% of that in WT females, this was not significantly different (*P*=0.535; Fig 4D). In addition, the marked sexual dimorphism in LH content seen in WT mice (*P*<0.0001) was not replicated in PWS-IC^{del} littermates (*P*=0.412). These differences in LH content remained after correction for protein content (*P*<0.05; data not shown).

Circulating IGF-1 was reduced in male and female PWS-IC^{del} mice by 47% and 37% respectively (*P*<0.0001 and P<0.001; Fig 5B). Although mean plasma LH and FSH concentration in PWS-IC^{del} males were 163% and 123% of that in male WT littermates, these were not significantly different (*P*>0.900; Fig 5C & D). Plasma LH and FSH concentrations were comparable in WT and PWS-IC^{del} females and there was no sexual dimorphism in circulating gonadotrophin levels in either genotype (Fig 5C & D).

Study 4. The effect of thermoneutrality on skeletal parameters in PWS-IC^{del} mice

As in study 1, tibial length in male PWS-IC^{del} mice at standard ambient temperature were reduced by 11% (*P*<0.0001; Fig 6A), with a similar (10%) reduction in females (*P*<0.0001; data not shown). This difference was maintained at thermoneutrality in males (9% reduction; *P*<0.001; Fig 6A) and females (8% reduction; *P*<0.0001), thermoneutrality having no effect on either tibial length nor EPW in either genotype (Fig 6A & B).

Mean tibial marrow adiposity and adipocyte number in PWS-IC^{del} mice at standard ambient temperature were only 22% and 29% of that in WT males, but given the variation in the WT data, these were not statistically different (*P*=0.5668 (adiposity); Fig 6C; *P*=0.3388 (adipocyte number); Fig 6D). Thermoneutrality had no statistically significant effect on tibial marrow adiposity (Fig 6C) or adipocyte size in either WT or PWS-IC^{del} males (Fig 6E). Parallel results were also obtained in females (data not

 Accepted Manuscript published as JOE-19-0279.R1. Accepted for publication: 19-Aug-2019

shown). Analysis of the adipocyte size profile revealed that while differences were seen between PWS-IC^{del} males and their WT littermates at room temperature (e.g. there were less adipocytes in the size range 525-572µm^2 in PWS-IC^{del} mice (Fig 6F; P=0.038)), these differences were abolished in mice maintained at thermoneutrality (Fig 6G).

As above, femoral length and cortical diameter were reduced by 8% and 25% in male PWS-IC^{del} mice at 20-22°C (P<0.0001; Fig 7A & B), with average cortical wall thickness not being significantly different (Fig 7C). None of these geometric variables were altered by increasing the ambient temperature to thermoneutrality (Fig 7A-C). However, the 48% reduction in the biomechanical strength of the femoral cortex in PWS-IC^{del} mice at room temperature (P<0.0001; Fig 7D), was abolished when PWS-IC^{del} mice were maintained at thermoneutrality (Fig 7D). This improvement in biomechanical performance was entirely due to the significant increase in the strength of the calcified tissue, UTS in PWS-IC^{del} mice at 30°C being 91% higher than in WT littermates at thermoneutrality (P<0.01; Fig 7E). In the absence of any significant effect of thermoneutrality on femoral geometry, there was no change in the geometric contribution to strength, which remained at 32% of that in WT mice (Fig 7F). Similar results were obtained in females, the impaired biomechanical strength in PWS-IC^{del} mice at 20-22°C (P=0.007), being ameliorated at thermoneutrality (P=0.215), as a consequence of the contribution of tissue strength, the impaired geometric contribution being exacerbated (P=0.006) (data not shown).

Discussion

Loss of gene expression from the paternal allele of chromosome 15q11-q13 results in the marked disturbances in neural development, hormone secretion and metabolic homeostasis that characterise PWS. However, despite impaired GH secretion and GH replacement long being considered a key feature of this condition and an important element in therapeutic strategy (Lee et al, 1987; Deal et al, 2013; Carias & Wevrick, 2019), our understanding of the significance of GH-deficiency for skeletal growth and integrity in the preclinical animal models of PWS is surprisingly superficial. To address this gap in our knowledge, we have analysed the phenotype of the weight-bearing long bones of the PWS-IC^{del} mouse model for "full" PWS, shedding new light on the mechanisms of fracture risk in this complex condition.

Three prominent features of the observed skeletal phenotype deserve comment: impaired morphometric growth, impaired marrow adiposity and impaired biomechanical strength.

Preliminary evidence of growth retardation has been reported in most of the murine models for PWS, including mice with uniparental disomy (Cattanach et al, 1992) and deletions of *Snrpn-Ube3a* (Tsai et al, 1999a), *Snurf/Snrpn exon 2* (Tsai et al, 1999b), *Snord116* (Ding et al, 2008) and *Magel2* (Bischof et al, 2007; Baraghithy, 2019), with *Necdin*^{del} mice showing normal growth (Tsai et al, 1999a). However, initial attempts to quantify skeletal growth following IC deletion, in which expression of all the genes in the PWS locus is lost, have been hampered by high neonatal mortality (Yang et al, 1998). Having developed a breeding strategy to partially overcome this problem, we now report that PWS-IC^{del} mice display consistent shortening of appendicular bones.

 Accepted Manuscript published as JOE-19-0279.R1. Accepted for publication: 19-Aug-2019

This growth impairment is most likely to result from the marked deficiency in the GH-IGF-1 axis (40-50% reductions in both pituitary GH content and circulating IGF-1). Although we cannot exclude a potential reduction in GH sensitivity, it is evident from comparison with other murine models for isolated GH-deficiency (GH-D) or reduced GH signalling that the degree of growth retardation in mice appears to reflect the severity of axis inactivation, with complete loss of GH secretion/signalling producing the most severe phenotype (20-25% reduction in body length; Alba and Salvatori, 2004; Zhou *et al*, 1997; Stevenson *et al*, 2009).

It is important to note, however, that femoral diameter (reduced by 32% in PWS-IC^{del} mice) was more profoundly affected than longitudinal growth. This occurred without affecting cortical wall thickness. Although broadly similar findings in mice with reduced GH signalling (Stevenson *et al*, 2009) suggest that loss of GH activity may be an important determinant, the fact that cortical diameter is only reduced by 17% in the complete absence of GH-receptors implies that other factors in the PWS endotype may contribute to this diminution of diameter.

While GH-deficiency may be the most likely cause, we cannot exclude the potentially negative influence of gonadotropin deficiency on bone formation (Yarram *et al*, 2003). In contrast, the observed PRL-deficiency is unlikely to represent a significant factor in this context as PRL has been shown to inhibit osteoblast function (Cross *et al*, 2000). However, given the growing evidence for impaired oxytocin signalling in mouse models for PWS (Schaller *et al*, 2010), further analysis should investigate the potentially negative impact of oxytocin loss on the skeletal phenotype (Elabd *et al*, 2008).

A potential physical mechanism relates to the marked reduction in body weight (reduced by 40%) and adiposity (individual fat pad weights reduced by 67-84%) seen in PWS-IC^{del} mice (Golding *et al*, 2017). This leanness has a number of consequences. Firstly, the loading forces being applied to these weight bearing bones are significantly reduced. These forces promote the remodelling of the bone to enhance diameter and weight-bearing capacity (David *et al*, 2007; Luu *et al*, 2009). Although muscle mass was not quantified in the current study, muscle hypoplasia in the *Magel2*^{del} mouse model for PWS/Schaaf-Yang syndrome (SYS) (Kamaludin *et al*, 2016), indicates that this could represent a possible transduction mechanism. Secondly, such profound reductions in abdominal fat mass are likely to cause a dramatic reduction in circulating leptin. Any effect of hypoleptinaemia is likely to be enhanced by changes in the marrow milieu resulting from the equally dramatic reduction in marrow adiposity in this model.

This marked decline in tibial marrow adiposity is due to reductions in both marrow adipocyte number and size. While the latter parallels the changes we previously reported in intra-abdominal white adipose tissue (Golding *et al*, 2017), our current data indicates that in the bone marrow at least, impaired adipogenesis is also a significant factor. In the context of the barrage of endocrine signals promoting marrow adiposity, this is quite remarkable. For example, *dw/dw* rats, which show a similar degree of GH-D accompanied by intra-abdominal leanness, show elevated marrow adiposity (mainly increased adipogenesis) (Gevers *et al*, 2002), with GH treatment inhibiting adipogenesis and triglyceride storage (Gevers *et al*, 2002). In addition, since ghrelin is powerfully adipogenic in bone marrow (Thompson *et al*, 2004; Davies *et al*, 2009; Hopkins et al, 2017), the marked hyperghrelinaemia in PWS-IC^{del} mice (Golding *et al*, 2017) should elevate marrow adiposity. Clearly, the anti-adipogenic signals in PWS-IC^{del} mice are more than sufficient to reverse these influences. The absence of the larger adipocytes in

 Accepted Manuscript published as JOE-19-0279.R1. Accepted for publication: 19-Aug-2019

bone marrow corresponds with the reported impairment of lipid storage capacity in intra-abdominal WAT in these mice (Golding *et al*, 2017) and the impairment of lipid storage in cultured adipocytes from humans with PWS (Cadoudal *et al*, 2014). Whether the obesity that usually accompanies PWS in humans leads to parallel changes in marrow adiposity remains to be established.

With this degree of leanness in the marrow, it is highly likely that the production of leptin from marrow adipocytes (Laharrague *et al*, 1998) is reduced in parallel. Interestingly, intra-bone marrow infusion of leptin in GH-D rats not only halves marrow adiposity by suppressing adipogenesis, but increases osteoblast surface (Evans et al, 2011). Given this role of leptin in maintaining the bone microenvironment, one would expect bones from PWS-IC^{del} mice to show evidence of elevated osteoblast activity. However, while the function of PWS-IC^{del} osteoblasts should be examined *in vitro*, our data indicate that osteoblast activity does not appear to be enhanced *in vivo*. Indeed, the combination of unaltered relative trabecular surface, a more fragmented trabecular lattice and an unchanged osteoclast density, imply that PWS-IC^{del} osteoblast number and/or activity is reduced. The combined reduction in adipocytes and osteoblasts is unusual and suggests a failure in the proliferation of MSCs or their subsequent differentiation.

In the context of this endocrine and cellular milieu, the biomechanical integrity of the femoral cortex is clearly compromised. Surprisingly, UTS, a measure of the strength of the calcified tissue, *per se*, is significantly increased. Such increases in tissue strength usually result from a greater density of either matrix proteins or hydroxyapatite. This is likely to be due to the reduction in GH-axis activity, producing slower growing and less remodelled bone (Locatelli & Bianchi, 2014). Nevertheless, despite this increased tissue strength, the geometric component of strength (second moment of area) is profoundly reduced, which corresponds directly with the smaller cortical diameter discussed above. Indeed, the impairment of this geometric component is more than sufficient to translate an elevated UTS into a compromised overall organ strength.

While the analysis of single-gene deletion models in this context is far from complete, the information available suggests some potential genetic mechanisms underlying the complex skeletal phenotype observed. The impairment of the GH-axis may be due in part to the loss of expression of Snord116, because although *Snord116*^{del} mice show normal pituitary volume, somatotroph number (Ding *et al*, 2008) and GH content (Burnett *et al*, 2017), circulating IGF-1 is reduced by 60-70% (Ding *et al*, 2008; Qi *et al*, 2016). This lack of GH action, possibly as the result of impaired activity of the hormone pro-convertase enzyme PC1 (Burnett *et al*, 2017) increases GH-releasing hormone mRNA expression in the arcuate nucleus (Qi *et al*, 2016) reflecting impaired GH feedback. In contrast, male *Magel2*^{del} mice show normal IGF-1 levels, with IGF-1 secretion and ghrelin-induced (but not GHRH-induced) GH responses impaired in female mice (Tennese & Wevrick, 2011). However, given the episodic nature of GH secretion in rodents, establishing the relationship between these specific genes and the parameters of spontaneous GH secretion would be more readily achieved in a larger species.

In the context of skeletal growth, body length is only modestly reduced in *Snord116*^{del} mice, with a 10% reduction in bone mineral density (Ding *et al*, 2008; Qi *et al*, 2016). Although overall body length is normal in the absence of *Magel2* (Bischof et al, 2007), femoral length, cortical diameter and cortical wall thickness are reduced in female *Magel2*^{del} mice by 9-13% (Baraghithy *et al*, 2019). Indeed, this is the only model in which a comprehensive analysis has been made of the skeletal phenotype. Interestingly, although these mice also show comparable reductions in trabecular number, trabecular fragmentation, femoral strength and UTS to that reported here in the PWS-IC*del* mice, marrow adiposity is more than doubled (Baraghithy *et al*, 2019) compared to the profound reduction reported here. This implies that loss of one of the other genes in the PWS locus either disrupts the relationship between adipocyte and osteoblast differentiation, or the proliferation of MSCs. Since *Necdin* has already been identified as a regulator of astrocyte (Fujimoto et al, 2016), neocortical neural precursor cell (Minamide et al, 2014), hematopoietic stem cell (Asai et al, 2012) and pre-adipocyte (Fujiwara *et al*, 2012) differentiation, this seems like a potential candidate.

Given that the normal relationship between fat mass and bone remodelling is disrupted in PWS-IC*del* mice, and our previous evidence that raising ambient temperature suppresses brown adipose tissue function (Golding *et al*, 2017), we investigated the effects of maintaining PWS-IC*del* mice at thermoneutrality on this altered skeletal phenotype. While this manipulation had no effect on marrow adiposity, there was a significant improvement in biomechanical strength as a result of an increased strength of the calcified tissue. This is remarkable since we have previously shown that this manipulation halved food intake in PWS-IC*del* mice (Golding *et al*, 2017). When coupled with evidence that thermoneutrality normalises skeletal length and bone mineral density in Snord116*del* mice (Qi et al, 2017), this implies that bone turnover is dramatically reduced at thermoneutrality. This interpretation is supported by evidence that thermoneutrality increases bone formation and reduces bone resorption in growing female C17BL/6J mice, while dramatically reducing food intake and doubling marrow adiposity (Iwaniec et al, 2016). The latter observation serves to re-emphasize the likely impairment of adipocyte function in the PWS-IC*del* model (Golding *et al*, 2017).

In summary, our data show that the longitudinal growth and biomechanical integrity of long bones are markedly impaired in the PWS-IC*del* mouse model for “full” PWS. Whether this impairment is matched by deficits in the biomechanical properties of other types of bone, e.g. calvarial or vertebral bone, has yet to be established, but our data not only provide a biomechanical basis for the increased fracture risk in PWS (Butler *et al*, 2002; Longhi *et al*, 2015), but indicate that thermoneutrality may be beneficial in this context. The final phenotype observed in the PWS-IC*del* mice appears to result from the combined loss of several genes from within the PWS locus, but a more precise genetic cause for the individual aspects remains to be fully elucidated.

 Accepted Manuscript published as JOE-19-0279.R1. Accepted for publication: 19-Aug-2019

References

Alba M & Salvatori R 2004 A mouse with targeted ablation of the growth hormone-releasing hormone gene: a new model of isolated growth hormone deficiency. *Endocrinology* **145** 4134-4143. (doi: https://doi.org/10.1210/en.2004-0119)

Asai T, Liu Y, Di Giandomenico S, Bae N, Ndiaye-Lobry D, Deblasio A, Menendez S, AntipinY, Reva B, Wevrick R *et al* 2012 Necdin, a P53 target gene, regulates the quiescence and response to genotoxic stress if hematopoietic stem/progenitor cells. *Blood* **120** 1601-1612. (doi: 10.1182/blood-2011-11-393983)

Baraghithy S, Smoum R, Drori A, Hdar R, Gammal, A, Hirsch S, Attar-Namdar M, Nemirovski A, Gabet Y, Langer Y *et al* 2019 *Magel2* modulates bone remodelling and mass in Prader-Willi syndrome by affecting oleoyl serine levels and activity. *Journal of Bone and Mineral Research* **34** 93-105 (doi: https://doi.org/10.1002/jbmr.3591)

Beresford JN, Bennett JH, Devlin C, Leboy PS & Owen ME 1992 Evidence for an inverse relationship between the differentiation of adipocytic and osteogenic cells in rat marrow stromal cell cultures. *Journal of Cell Science* **102** 341-351. (PMID: 1400636)

Bischof JM, Stewart CL & Wevrick R 2007 Inactivation of the mouse *Magel2* gene results in growth abnormalities similar to Prader-Willi syndrome. *Human Molecular Genetics* **16** 2713-2719. (doi: 10.1093/hmg/ddm225)

Bouxsein ML, Boyd SK, Christiansen BA, Guldberg RE, Jepsen KJ & Müller R 2010 Guidelines for assessment of bone microarchitecture in rodents using micro-computed tomography. *Journal of Bone and Mineral Research* **25** 1468-1486 (doi: 10.1002/jbmr.141)

Burnett LC, LeDuc CA, Sulsona CR, Paul D, Rausch R, Eddiry A, Martin Carli JF, Morabito MV, Skowronski AA, Hubner G *et al* 2017 Deficiency in prohormone convertase PC1 impairs prohormone processing in Prader-Willi syndrome. *Journal of Clinical Investigation* **127** 293-305. (doi: 10.1172/JCI88648)

Butler JV, Whittington JE, Holland AJ, Boer H, Clarke D & Webb T 2002 Prevalence of, and risk factors for, physical ill-health in people with Prader-Willi syndrome: a population-based study. *Developmental Medicine and Child Neurology* **44** 248-255 (doi: https://doi.org/10.1017/S001216220100202X)

Butler MG, Manzardo AM & Forster JL 2016 Prader-Willi syndrome: clinical genetics and diagnostic aspects with treatment approaches. *Current Pediatric Reviews* **12** 136-166. (doi: 10.2174/1573396312666151123115250)

Cadoudal T, Buléon M, Segenès C, Diene G, Desneulin F, Molinas C, Eddiry S, Conte-Auriol F, Daviaud D, Martin PG *et al*. 2014 Impairment of adipose tissue in Prader-Willi syndrome rescued by growth hormone treatment. *International Journal of Obesity (London)* **38** 1234-1240. (doi: 10.1038/ijo.2014.3)

Carias KV & Wevrick R 2019 Preclinical testing in translational animal models of Prader-Willi syndrome: overview and gap analysis. *Molecular Therapy: Methods & Clinical Assessment* **13** 344-358. (doi: https://doi.org/10.1016/j.omtm.2019.03.001)

Cattanach BM, Barr JA, Evans EP, Burtenshaw M, Beechey CV, Leff SE, Brannan CI, Copeland NG, Jenkins NA & Jones J 1992 A candidate mouse model for Prader-Willi syndrome which shows an absence of Snrpn expression. *Nature Genetics* **2** 270-274. (doi: 10.1038/ng1292-270)

Chamberlain SJ, Johnstone KA, DuBose AJ, Simon TA, Bartolomei MS, Resnick JL & Brannan CI 2004 Evidence for genetic modifiers of postnatal lethality in PWS-IC deletion mice. *Human Molecular Genetics* **13** 2971-2977. (doi: 10.1093/hmg/ddh314)

Cross D, Yang Y, Kuo CB, Xu X, Luben RA & Walker AM 2000 Effects of prolactin on osteoblast alkaline phosphatase and bone formation in the developing rat. *American Journal of Physiology Endocrinology and Metabolism* **279** E1216-E1226. (doi: 10.1152/ajpendo.2000.279.6.E1216)

Cummings DE, Clement K, Purnell JQ, Vaisse C, Foster KE, Frayo RS, Schwartz MW, Basdevant A & Weigle DS 2002 Elevated plasma ghrelin levels in Prader-Willi syndrome. *Nature Medicine* **8** 643-644. (doi: 10.1038/nm0702-643)

David V, Martin A, Lafage-Proust M-H, Malaval L, Peyroche S, Jones DB, Vico L & Guignandon A 2007 Mechanical loading down-regulates peroxisome proliferator-activated receptor γ in bone marrow stromal cells and favours osteoblastogenesis at the expense of adipogenesis. *Endocrinology* **148** 2553-2562. (doi: 10.1210/en.2006-1704)

Davies JS, Kotokorpi P, Eccles SR, Barnes SK, Tokarczuk PF, Allen SK, Whitworth HS, Guschina IA, Evans BA, Mode A *et al* 2009 Ghrelin induces abdominal obesity via GHS-R-dependent lipid retention. *Molecular Endocrinology* **23** 914-924. (doi: 10.1210/me.2008-0432)

Deal CL, Tony M, Höybye C, Allen DB, Tauber M, Christiansen JS, and the 2011 Growth Hormone in Prader-Willi Syndrome Clinical Care Guidelines Workshop Participants 2013. Growth Hormone Research Society Workshop Summary: consensus guidelines for recombinant human growth hormone therapy in Prader-Willi syndrome. *Journal of Clinical Endocrinology and Metabolism* **98** E1072-E1087. (doi: 10.1210/jc.2012-3888)

Di Iorgi, Rosol M, Mittelman SD & Gilsanz V 2008 Reciprocal relation between marrow adiposity and the amount of bone in the axial and appendicular skeleton of young adults. *Journal of Clinical Endocrinology and Metabolism* **93** 2281-2286. (doi: 10.1210/jc.2007-2691)

Ding F, Li HH, Zhang S, Solomon NM, Camper SA, Cohen P & Franke U 2008 SnoRNA Snord116 (Pwcr/MBII-85) deletion causes growth deficiency and hyperphagia in mice. *PLoS One* **3** 31709. (doi: 10.1371/journal.pone.0001709).

Elabd C, Basillais A, Beaupied H, Breuil V, Wagner N, Scheideler M, Zaragosi LE, Massiéra F, Lemichez E, Benhamou CL, Dani C, Amri EZ 2008 Oxytocin controls differentiation of human mesenchymal stem cells and reverses osteoporosis. *Stem Cells* **26** 2399-2407. (doi: 10.1634/stemcells.2008-0127)

Evans BAJ, Bull MJ, Kench RC, Fox RE, Morgan LD, Stevenson AE, Gevers EF, Perry MJ & Wells T 2011 The influence of leptin on trabecular architecture and marrow adiposity in GH-deficient rats. *Journal of Endocrinology* **208** 69-79. (doi: 10.1677/JOE-10-0178)

Fujimoto I, Hasegawa K, Fujiwara K, Yamada M & Yoshikawa K 2016 Necdin controls EGFR signalling linked to astrocyte differentiation in primary cortical progenitor cells. *Cellular Signalling* **28** 94-017. (doi: 10.1016/j.cellsig.2015.11.016)

Fujiwara K, Hasegwa K, Ohkumo T, Miyoshi H, Tseng YH & Yoshikawa K 2012 Necdin controls proliferation of white adipose progenitor cells. *PLoS One* **7** e30948. (doi: 10.1371/journal.pone.0030948)

Gevers EF, Loveridge N & Robinson IC 2002 Bone marrow adipocytes: a neglected target tissue for growth hormone. *Endocrinology* **143** 4065-4073. (doi: 10.1210/en.2002-220428)

Golding DM, Rees DJ, Davies JR, Relkovic D, Furby HV, Guschina IA, Davies JS, Resnick JL, Isles AR & Wells T. 2017. Paradoxical leanness in the imprinting-centre deletion mouse model for Prader-Willi syndrome. *Journal of Endocrinology* **232** 123-135. (doi: 10.1530/JOE-16-0367)

Grosso S, Cioni M, Peruzzi L, Pucci L & Berardi R 1998 Growth hormone secretion in Prader-Willi syndrome. *Journal of Endocrinological Investigation* **21** 418-422. (doi: 10.1007/BF03347319)

Guillou A, Romanò N, Steyn F, Abitbol K, Le Tissier P, Bonnefont X, Chen C, Mollard P & Martin AO. 2015. Assessment of lactotroph axis functionality in mice: longitudinal monitoring of PRL secretion by ultrasensitive-ELISA. *Endocrinology* **156**:1924-30. (doi: 10.1210/en.2014-1571)

Hamrick MW, Della-Fera MA, Choi Y-H, Pennington C, Hartzell D & Baile CA 2005 Leptin treatment induces loss of bone marrow adipocytes and increases bone formation in leptin-deficient *ob/ob* mice. *Journal of Bone and Mineral Research* **20** 994-1001. (doi: 10.1359/JBMR.050103)

Hopkins AL, Nelson TAS, Guschina IA, Parsons LC, Lewis CL, Brown RC, Christian HC, Davies JS & Wells T 2017 Unacylated ghrelin promotes adipogenesis in rodent bone marrow via ghrelin *O*-acyl transferase and GHS-R_{1a} activity: evidence for target cell-mediated acylation. *Scientific Reports* **7** 45541. (doi: 10.1038/srep45541)

Iwaniec UT, Philbrick KA, Wong CP, Gordon JL, Kahler-Quesada AM, Olson DA, Branscum AJ, Sargent JL, DeMambro VE, Rosen CJ *et al*. 2016. Room temperature housing results in premature cancellous bone loss in growing female mice: implications for the mouse as a preclinical model for age-related bone loss. Osteoporosis International 27 3091-3101 (doi: 10.1007/s00198-016-3634-3)

Kamaludin AA, Smolarchuk C, Bischof JM, Eggert R, Greer JJ, Ren J, Lee JJ, Yokota T, Berry FB & Wevrick R 2016 Muscle dysfunction caused by loss of Magel2 in a mouse model of Prader-Willi and Schaaf-Yang syndromes. *Human Molecular Genetics* **25** 3798-3809. (doi: 10.1093/hmg/ddw225)

Kahn MJ, Gerasimidis K, Edwards CA & Shaikh MG 2018 Mechanisms of obesity in Prader-Willi syndrome. *Pediatric Obesity* **13** 3-13. (doi: 10.1111/ijpo.12177)

Khor EC, Fanshawe B, Qi Y, Zolotukhin S, Kulkarni RN, Enriquez RF, Purtell L, Lee NJ, Wee NK, Croucher PI, Campbell L *et al*. 2016 Prader-Willi critical region, a non-translated, imprinted central regulator of bone mass: possible role in skeletal abnormalities on Prader-Willi syndrome. *PLoS One* **11** e0148155. (10.1371/journal.pone.0148155)

Laharrague P, Larrouy D, Fontanilles AM, Truel M, Campfield A, Tenenbaum R, Galitzky J, Corberand JX, Pénicaud L & Casteilla L 1998 High expression of leptin by human bone marrow adipocytes in primary culture. *FASEB Journal* **12** 747-752. (PMID: 9619453)

Lee PD, Wilson DM, Rountree L, Hintz RL & Rosenfeld RG. 1987. Linear growth response to exogenous growth hormone in Prader-Willi syndrome. *American Journal of Medical Genetics* **28** 865-871. (doi: 10.1002/ajmg.1320280411)

Leiben L, Callewaert F & Bouillon R 2009 Bone and metabolism: a complex crosstalk. *Hormone Research* **71** (**Suppl 1**) 134-138. (doi: https://doi.org/10.1159/000178056)

Locatelli V & Bianchi VE 2014 Effect of GH/IGF-1 on bone metabolism and osteoporosis. *International Journal of Endocrinology* **2014** 235060. (doi: 10.1155/2014/235060)

Longhi S, Grugni G, Gatti D, Spinnozzi E, Sartorio A, Adami S, Fanolla A & Radetti G 2015 Adults with Prader-Willi syndrome have weaker bones: effect of treatment with GH and sex steroids. *Calcified Tissue International* **96** 160-166. (doi: 10.1007/s00223-014-9949-1)

Luu YK, Capilla E, Rosen CJ, Gilsanz V, Pessin JE, Judex S & Rubin CT 2009 Mechanical stimulation of mesenchymal stem cell proliferation and differentiation promotes osteogenesis while preventing dietary-induced obesity. *Journal of Bone and Mineral Research* **24** 50-61. (doi: 10.1359/JBMR.080817)

Miller JL, Lynn CH, Driscoll DC, Goldstone AP, Gold JA, Kimonis V, Dykens E, Butler MG, Shuster JJ & Driscoll DJ. 2011. Nutritional phases in Prader-Willi syndrome. *Am J Med Genet Part A* **155** 1040-1049. (doi: 10.1002/ajmg.a.33951)

Minamide R, Fujiwara K, Hasegawa K & Yoshikawa K 2014 Antagonistic interplay between necdin and Bmi1 controls proliferation of neural precursor cells in the embryonic mouse neocortex. *PLoS One* **9** e84460. (doi: 10.1371/journal.pone.0084460)

Muscatelli F, Abrous DN, Massacrier A, Boccaccio I, Le Moal M, Cau P & Cremer H 2000 Disruption of the mouse Necdin gene results in hypothalamic and behavioural alterations reminiscent of the human Prader-Willi syndrome. *Human Molecular Genetics* **9** 3101-3110. (doi: doi.org/10.1093/hmg/9.20.3101)

Navein AE, Cooke EJ, Davies JR, Smith TG, Wells LHM, Ohazama A, Healy C, Sharpe PT, Evans SL, Evans BAJ *et al* 2016. Disrupted mitochondrial function in the Opa3^{L122P}

Accepted Manuscript published as JOE-19-0279.R1. Accepted for publication: 19-Aug-2019

mouse model for Costeff Syndrome impairs skeletal integrity. *Human Molecular Genetics* **25**:2404-2416. (doi: 10.1093/hmg/ddw107)

Pravdivyi I, Ballanyi K, Colmers WF & Wevrick R 2015 Progressive postnatal decline in leptin sensitivity of arcuate hypothalamic neurons in the Magel2-null mouse model of Prader-Willi syndrome. *Human Molecular Genetics* **24** 5276-4283. (doi: 10.1093/hmg/ddv159)

Qi Y, Purtell L, Fu M, Lee NJ, Aepler J, Zhang L, Loh K, Enriquez RF, Baldock PA, Zolotukhin S *et al* 2016 Snord116 is critical in the regulation of food intake and body weight. *Scientific Reports* **6** 18614. (doi: 10.1038/srep18614)

Qi Y, Purtell L, Fu M, Sengmany K, Loh K, Zhang L, Zolotukhin S, Sainsbury A, Campbell L & Herzog H. 2017. Ambient temperature modulates the effects of the Prader-Willi syndrome candidate gene Snord116 on energy homeostasis. *Neuropeptides* **61** 87-93. (doi: 10.1016/j.npep.2016.10.006)

Schaller F, Watrin F, Sturny R, Massacrier A, Szepetowski P, Muscatelli F 2003 A single postnatal injection of oxytocin rescues the lethal feeding behaviour in mouse newborns deficient for the imprinted Magel2 gene. *Human Molecular Genetics* **19** 4895-4905. (doi: 10.1093/hmg/ddq424)

Stevenson AE, Evans BAJ, Gevers EF, McLeod RWJ, Perry MJ, El-Kasti MM, Coschigano KT, Kopchick JJ, Evans SL & Wells T. 2009. Does adiposity status influence femoral cortical strength in rodent models of growth hormone deficiency? *American Journal of Physiology Endocrinology and Metabolism* **296** E147-E156. (doi: 10.1152/ajpendo.90689.2008)

Steyn FJ, Huang L, Ngo ST, Leong JW, Tan HY, Xie TY, Parlow AF, Veldhuis JD, Waters MJ & Chen C 2011. Development of a method for the determination of pulsatile growth hormone secretion in mice. *Endocrinology* **152** 3165-3171. (doi: 10.1210/en.2011-0253)

Steyn FJ, Wan Y, Clarkson J, Veldhuis JD, Herbison AE & Chen C 2013. Development of a methodology for and assessment of pulsatile luteinizing hormone secretion in juvenile and adult male mice. *Endocrinology* **155** 4939-4945. (doi: 10.1210/en.2013-1502)

Tennese AA, Wevrick R 2011 Impaired hypothalamic regulation of endocrine function and delayed counterregulatory response to hypoglycaemia in Magel2-null mice. *Endocrinology* **152** 967-978. (doi: 10.1210/en.2010-0709)

Thomas T, Gori F, Khosla S, Jensen MD, Burguera B & Riggs BL 1999 Leptin acts on human marrow stromal cells to enhance differentiation to osteoblasts and to inhibit differentiation to adipocytes. *Endocrinology* **140** 1630-1638. (doi: https://doi.org/10.1210/endo.140.4.6637)

Thompson NM, Gill DAS, Davies R, Loveridge N, Houston PA & Robinson ICAF, Wells T 2004 Ghrelin and des-octanoyl ghrelin promote adipogenesis directly *in vivo* by a mechanism independent of the type 1a growth hormone secretagogue receptor. *Endocrinology* **145** 234-242. (doi: https://doi.org/10.1210/en.2003-0899)

Tilston TW, Brown RD, Wateridge MJ, Arms-Williams B, Walker JJ, Sun Y & Wells T 2019 A novel automated system yields reproducible temporal feeding patterns in laboratory rodents. *Journal of Nutrition* in press (doi: https://doi.org/10.1093/jn/nxz116)

Tsai TF, Armstrong D & Beaudet AL 1999a Necdin-deficient mice do not show lethality or the obesity and infertility of Prader-Willi syndrome. *Nature Genetics* **22** 15-16. (doi: 10.1038/8722)

Tsai TF, Jiang YH, Bressler J, Armstrong D & Beaudet AL 1999b Paternal deletion from Snrpn to Ube3a in the mouse causes hypotonia, growth retardation and partial lethality and provides evidence for a gene contributing to Prader-Willi syndrome. *Human Molecular Genetics* **8** 1357-1364. (doi: https://doi.org/10.1093/hmg/8.8.1357)

Yang T, Adamson TE, Resnick JL, Leff S, Wevrick R, Franke U, Jenkins NA, Copeland NG & Brannan CI 1998 A mouse model for Prader-Willi syndrome imprinting-centre mutations. Nature Genetics 19 25-31. (doi: 10.1038/ng0598-25)

Yarram SJ, Perry MJ, Christopher TJ, Westby K, Brown NL, Lamminen T, Rulli SB, Zhang FP, Huhtaniemi I, Sandy JR et al 2003 Luteinizing hormone receptor knockout (LuRKO) mice and transgenic human chorionic gonadotropin (hCG)-overexpressing mice (hCG alphabeta+) have bone phenotypes. *Endocrinology* **144** 3555-2564. (doi: 10.1210/en.2003-0036)

Zhou Y, Xu BC, Maheshwari HG, He L, Reed M, LozykowskiM, Okada S, Cataldo L, Coschigamo K, Wagner TE *et al* 1997 A mammalian model for Laron syndrome produced by targeted disruption of the mouse growth hormone receptor / binding protein gene (the Laron mouse). *Proceedings of the National Academy of Sciences (USA)* **94** 13215-13220. (doi: 10.1073/pnas.94.24.13215)

Accepted Manuscript published as JOE-19-0279.R1. Accepted for publication: 19-Aug-2019

Declaration of Interest

The authors declare that there is no conflict of interest that could be perceived as prejudicing the impartiality of the research reported.

Acknowledgments

The authors thank JBIOS staff and Derek Scarborough (Cardiff University) for excellent technical support.

Funding

This work was supported by a summer studentship awarded by the Foundation for Prader-Willi Research (to TMB, BEK and TW). AG and PM were supported by grants from the Agence Nationale de la Recherche (ANR-15-CE14-0012-01, ANR-18-C14-0017-01), Institut National de la Santé et de la Recherche Médicale, Centre National de la Recherche Scientifique, and Université de Montpellier.

Figure Legends

Figure 1: PWS-IC^{del} mice show impaired tibial growth and adiposity. Quantification of tibial length (A), in 18-month old male WT (n=6) and PWS-IC^{del} (n=6) littermate mice. Tibial epiphysial plate (EP) width (B) was quantified in Masson's Trichrome-stained sections and tibial marrow adiposity (C), marrow adipocyte number (D), size (E) and Size profile (F) quantified in digital images of Toluidene Blue-stained sections from WT (a) and PWS-IC^{del} (b) littermates. Osteoclast density (G) was quantified in TRAP^{+}-stained sections. Data shown are mean ± SEM (n=6 for both genotypes), with statistical comparisons performed by Student's unpaired T-test (*P<0.05; **P<0.01; ***P<0.001 vs WT littermates).

Figure 2: PWS-IC^{del} mice show impaired femoral morphology. Measurement of femoral length (A), outer cortical (anterior-posterior) diameter (A-P Ø; B) and average cortical wall thickness (C) in 18-month old male WT (n=6 (3 for B & C)) and PWS-IC^{del} (n=6) littermate mice. μ-CT was used to quantify the number (Tb.N; D), thickness (Tb.Th; E), cross-sectional shape (Structural modal (SM) index; F), relative surface (BS/BV; G), separation (Tb.Sp; H) and lattice fragmentation (Pattern factor; I) of trabeculae in the distal femora. Data shown are mean ± SEM, with statistical comparisons performed by Student's unpaired T-test (*P<0.05; **P<0.01 vs WT littermates).

Figure 3: PWS-IC^{del} mice show compromised femoral strength. Measurement of femoral strength (Ultimate moment; A), tissue strength (Ultimate tensile stress; B) and the geometric contribution to strength (Second moment of area; C) in 18-month old male WT (n=6 (3 for B & C)) and PWS-IC^{del} (n=6) littermate mice. Data shown are mean ±

 Accepted Manuscript published as JOE-19-0279.R1. Accepted for publication: 19-Aug-2019

SEM, with statistical comparisons performed by Student's unpaired T-test (**P*<0.05 vs WT littermates).

Figure 4: PWS-IC*del* mice show multiple pituitary hormone deficiencies. Quantification of weight (A) and growth hormone (GH; B), prolactin (PRL; C) and luteinising hormone (LH; D) contents in 6-15-month old male and female WT (n=6) and PWS-IC*del* (n=6 (male) and 5 (female)) littermate mice. Data shown are mean ± SEM, with statistical comparisons performed by 1-way ANOVA and Bonferroni post hoc test (**P*<0.05; ***P*<0.01; ****P*<0.001; *****P*<0.0001 vs WT littermates (same sex); ††P<0.01; †††† P<0.0001 vs male littermates (same genotype)).

Figure 5: PWS-IC*del* mice show reduced GH-IGF-1 axis activity. Quantification of pituitary weight (A) and plasma insulin-like growth factor-1 (IGF-1; B), luteinising hormone (LH; C) and follicle stimulating hormone (FSH; D) in 5-9-month old male and female WT and PWS-IC*del* (n=6 per group) littermate mice. Data shown are mean ± SEM, with statistical comparisons performed by 1-way ANOVA and Bonferroni post hoc test (A & B) or Kruskal-Wallis test (C & D) (****P*<0.001; *****P*<0.0001 vs WT littermates (same sex); †††† P<0.0001 vs male littermates (same genotype)).

Figure 6: Thermoneutrality has little effect on growth and marrow adiposity in PWS-IC*del* mice. Tibial length (A), epiphyseal plate (EP) width (B), marrow adiposity (C), marrow adipocyte number (D) and mean adipocyte size (E) were quantified in 6-15-month old male WT and PWS-IC*del* after being maintained at either standard ambient temperature (20-22°C) or thermoneutrality (30°C) for 9 weeks. Adipocyte size profiles are presented for standard ambient temperature (F) and thermoneutrality (G). Data shown are mean ± SEM (n=6 (room temperature) and 5 (thermoneutrality)), with

statistical comparisons performed by 1-way ANOVA and Bonferroni post hoc test (A-E; **** P<0.0001 vs room temperature (same genotype)) or unpaired Student's t-test (F & G; * P<0.05 vs WT littermates (same temperature)).

Figure 7: Thermoneutrality has little effect on growth and marrow adiposity in PWS-IC^{del} mice. Tibial length (A), epiphyseal plate (EP) width (B), marrow adiposity (C), marrow adipocyte number (D) and mean adipocyte size (E) were quantified in 6-15-month old male WT and PWS-IC^{del} after being maintained at either standard ambient temperature (20-22°C) or thermoneutrality (30°C) for 9 weeks (n=6 (room temperature) and 5 (thermoneutrality)). Data shown are mean ± SEM, with statistical comparisons performed by 1-way ANOVA and Bonferroni post hoc test (***P*<0.01; *****P*<0.0001 vs WT littermates (same ambient temperature)).

Accepted Manuscript published as JOE-19-0279.R1. Accepted for publication: 19-Aug-2019

Braxton TM *et al*, 2019; Figure 1

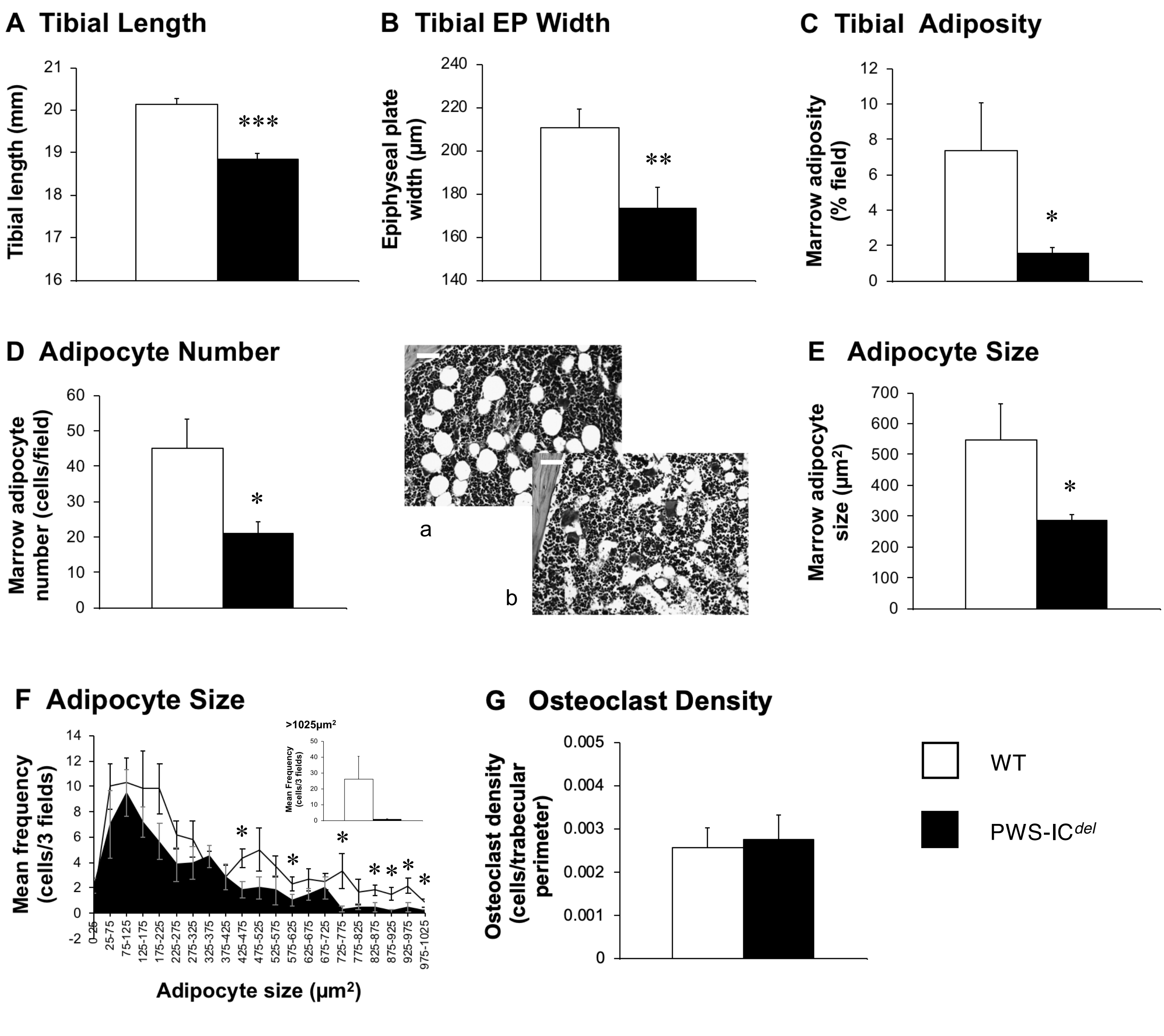

Figure 1: PWS-IC^{del} mice show impaired tibial growth and adiposity. Quantification of tibial length (A), in 18-month old male WT (n=6) and PWS-IC^{del} (n=6) littermate mice. Tibial epiphysial plate (EP) width (B) was quantified in Masson's Trichrome-stained sections and tibial marrow adiposity (C), adipocyte number (D), size (E) and Size profile (F) quantified in digital images of Toluidene Blue-stained sections from WT (a) and PWS-IC^{del} (b) littermates. Osteoclast density (G) was quantified in TRAP^{+}-stained sections. Data shown are mean ± SEM (n=6 for both genotypes), with statistical comparisons performed by Student's unpaired T-test (*P<0.05; **P<0.01; ***P<0.001 vs WT littermates).

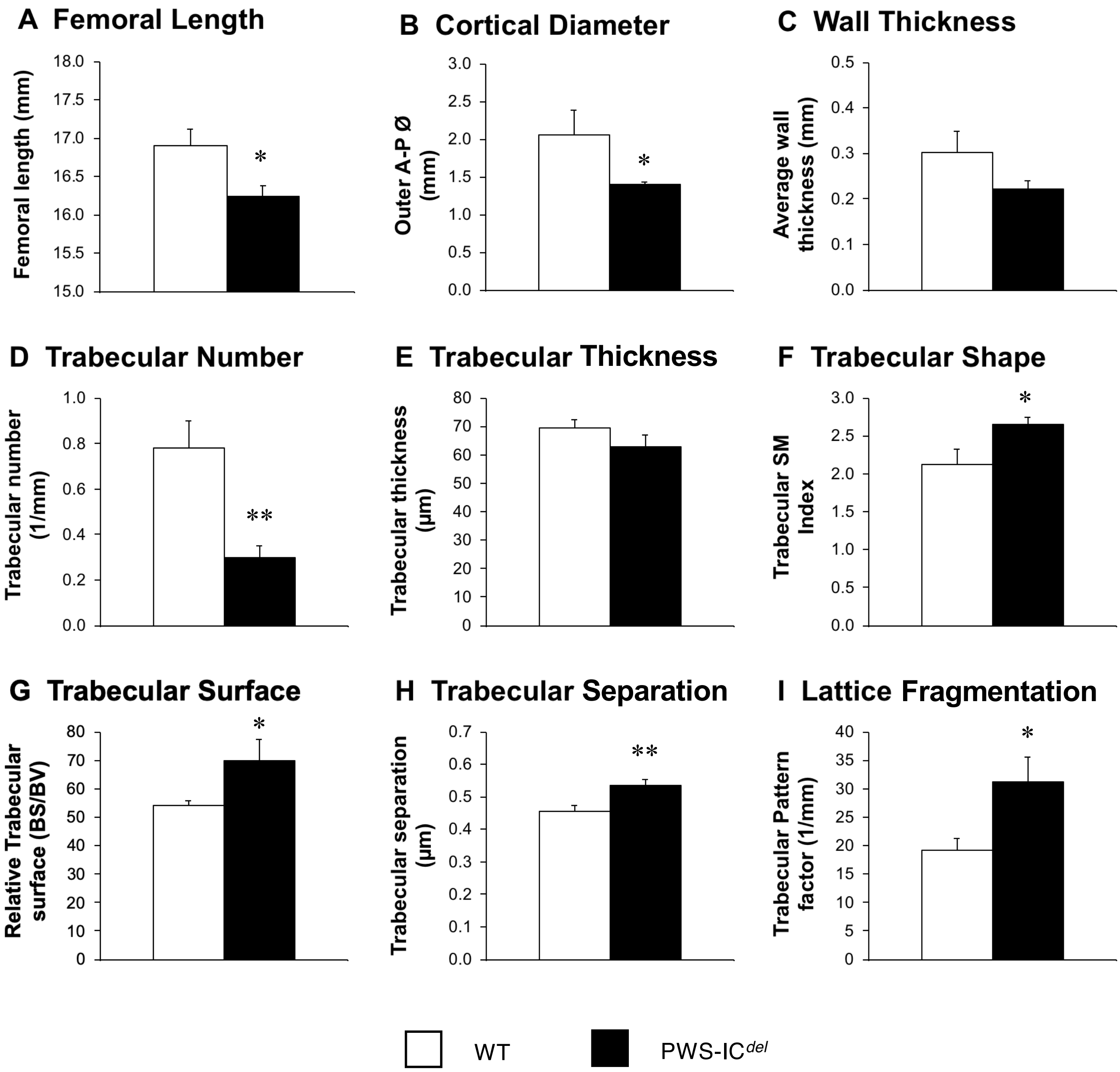

Figure 2: PWS-IC*del* mice show impaired femoral morphology. Measurement of femoral length (A), outer cortical (anterior-posterior) diameter (A-P Ø; B) and average cortical wall thickness (C) in 18-month old male WT (n=6 (3 for B & C)) and PWS-IC*del* (n=6) littermate mice. µ-CT was used to quantify the number (Tb.N; D), thickness (Tb.Th; E), cross-sectional shape (Structural modal (SM) index; F), relative surface (BS/BV; G), separation (Tb.Sp; H) and lattice fragmentation (Pattern factor; I) of trabeculae in the distal femora. Data shown are mean ± SEM, with statistical comparisons performed by Student's unpaired T-test (**P*<0.05; ***P*<0.01 vs WT littermates).

 Accepted Manuscript published as JOE-19-0279.R1. Accepted for publication: 19-Aug-2019

Braxton TM *et al*, 2019; Figure 3

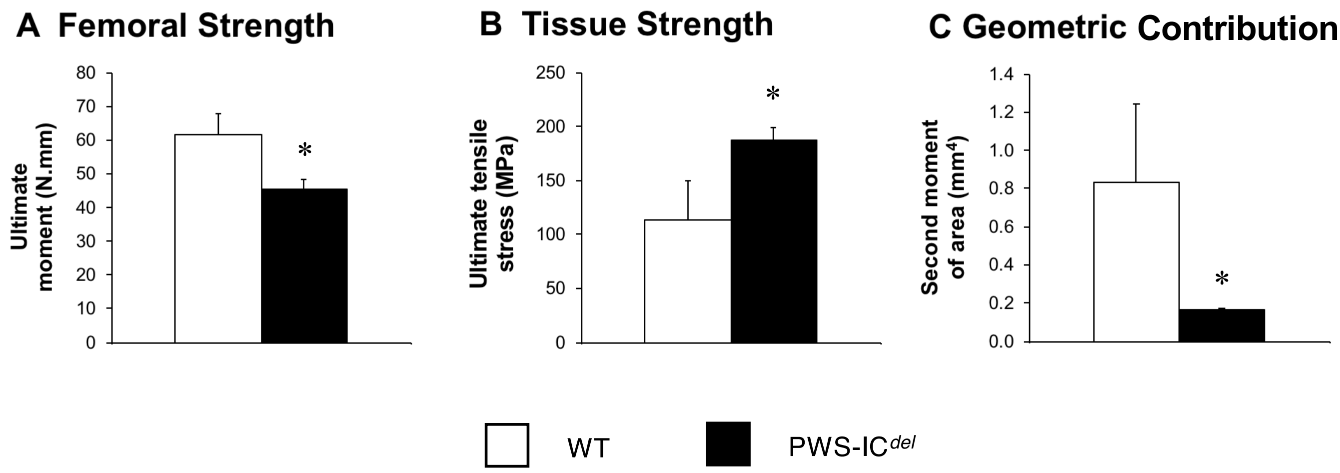

Figure 3: PWS-IC*del* mice show compromised femoral strength. Measurement of femoral strength (Ultimate moment; A), tissue strength (Ultimate tensile stress; B) and the geometric contribution to strength (Second moment of area; C) in 18-month old male WT (n=6 (3 for B & C)) and PWS-IC*del* (n=6) littermate mice. Data shown are mean ± SEM, with statistical comparisons performed by Student's unpaired T-test (**P*<0.05 vs WT littermates).

Braxton TM *et al*, 2019; Figure 4

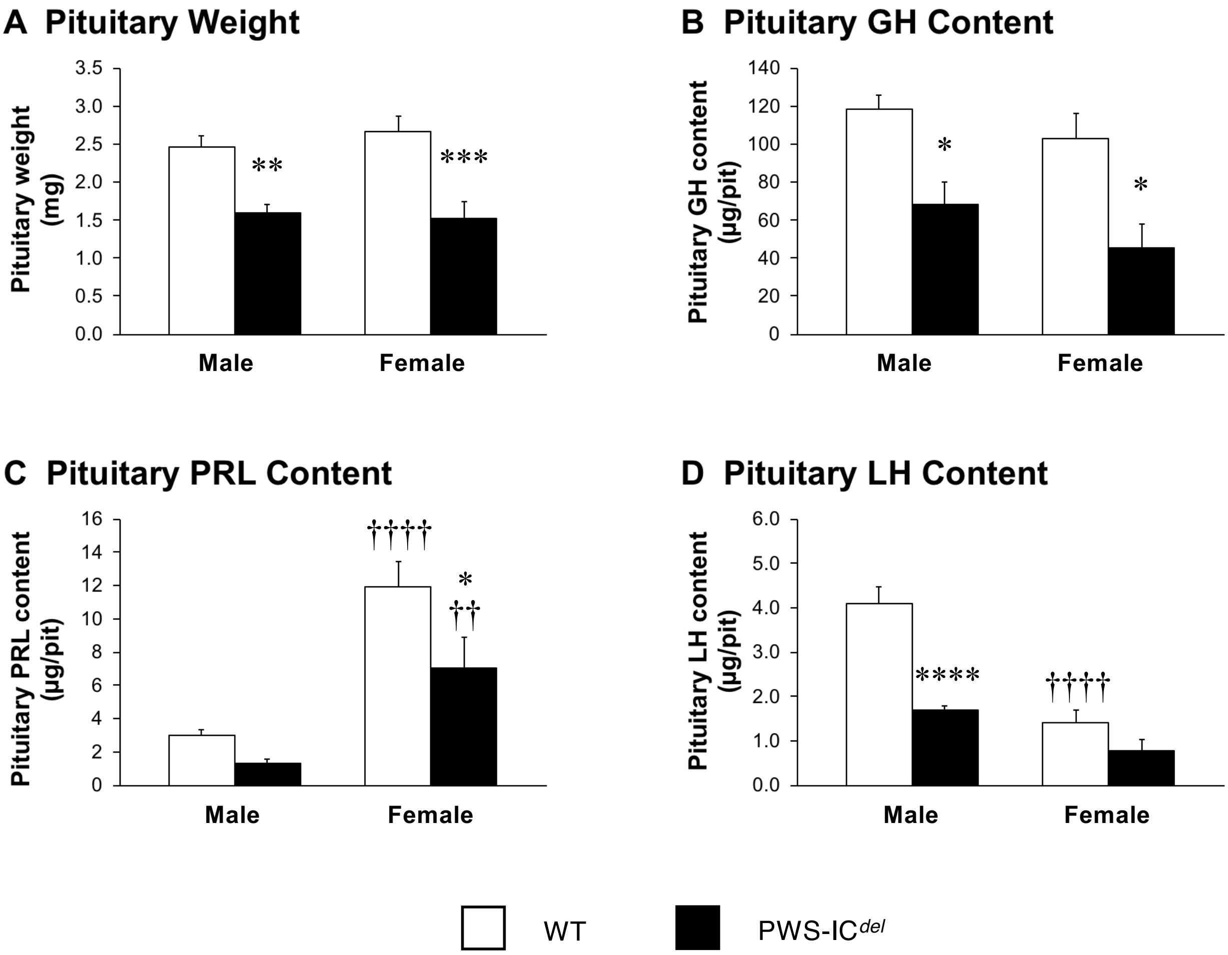

Figure 4: PWS-IC*del* mice show multiple pituitary hormone deficiencies. Quantification of weight (A) and growth hormone (GH; B), prolactin (PRL; C) and luteinising hormone (LH; D) contents in 6-15-month old male and female WT (n=6) and PWS-IC*del* (n=6 (male) and 5 (female)) littermate mice. Data shown are mean ± SEM, with statistical comparisons performed by 1-way ANOVA and Bonferroni post hoc test (*P<0.05; **P<0.01; ***P<0.001; ****P<0.0001 vs WT littermates (same sex); ††P<0.01; †††† P<0.0001 vs male littermates (same genotype)).

 Accepted Manuscript published as JOE-19-0279.R1. Accepted for publication: 19-Aug-2019

Braxton TM *et al*, 2019; Figure 5

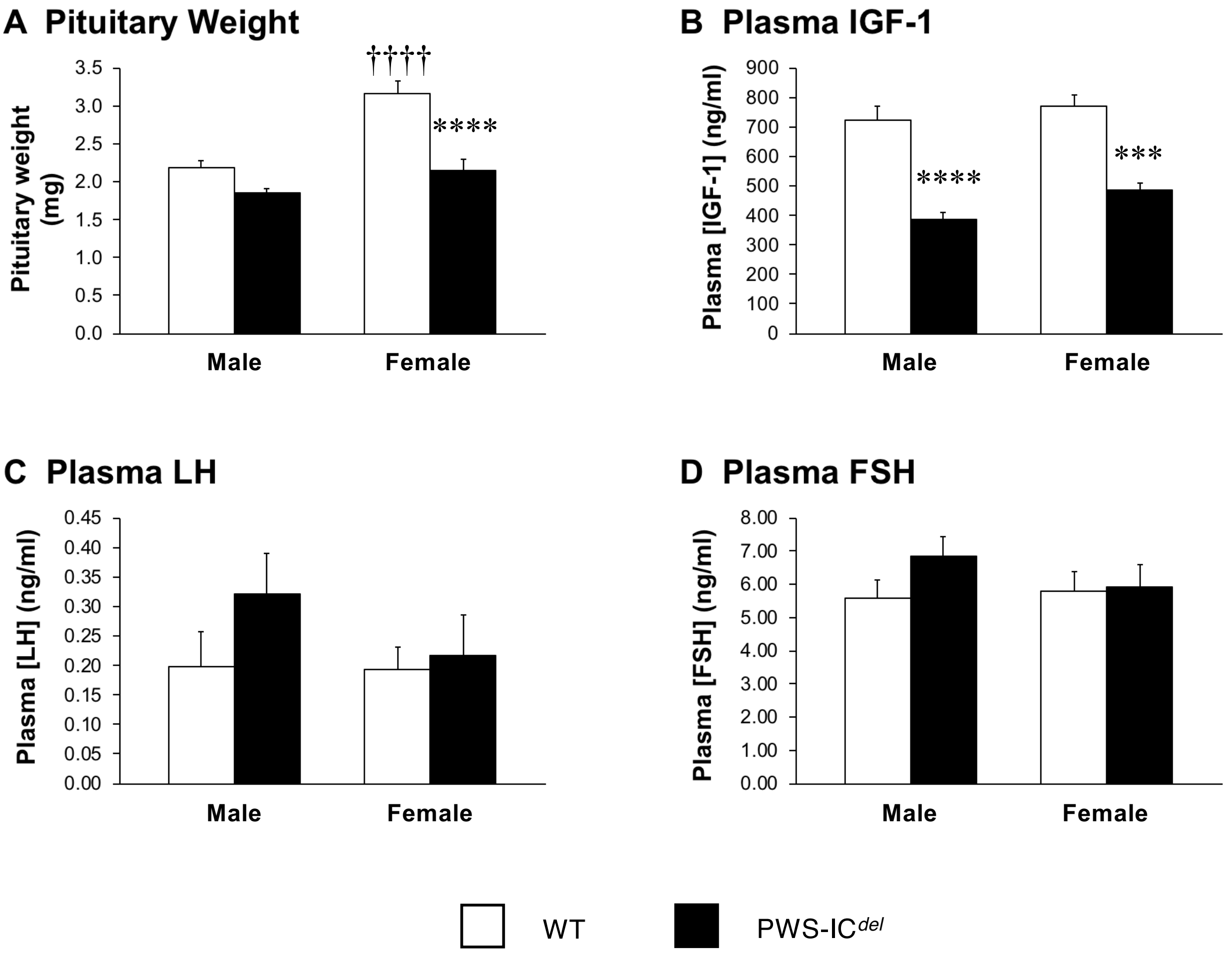

Figure 5: PWS-IC*del* mice show reduced GH-IGF-1 axis activity. Quantification of pituitary weight (A) and plasma insulin-like growth factor-1 (IGF-1; B), luteinising hormone (LH; C) and follicle stimulating hormone (FSH; D) in 5-9-month old male and female WT and PWS-IC*del* (n=6 per group) littermate mice. Data shown are mean ± SEM, with statistical comparisons performed by 1-way ANOVA and Bonferroni post hoc test (A & B) or Kruskal-Wallis test (C & D) (****P*<0.001; *****P*<0.0001 vs WT littermates (same sex); †††† P<0.0001 vs male littermates (same genotype)).

Braxton TM *et al*, 2019; Figure 6

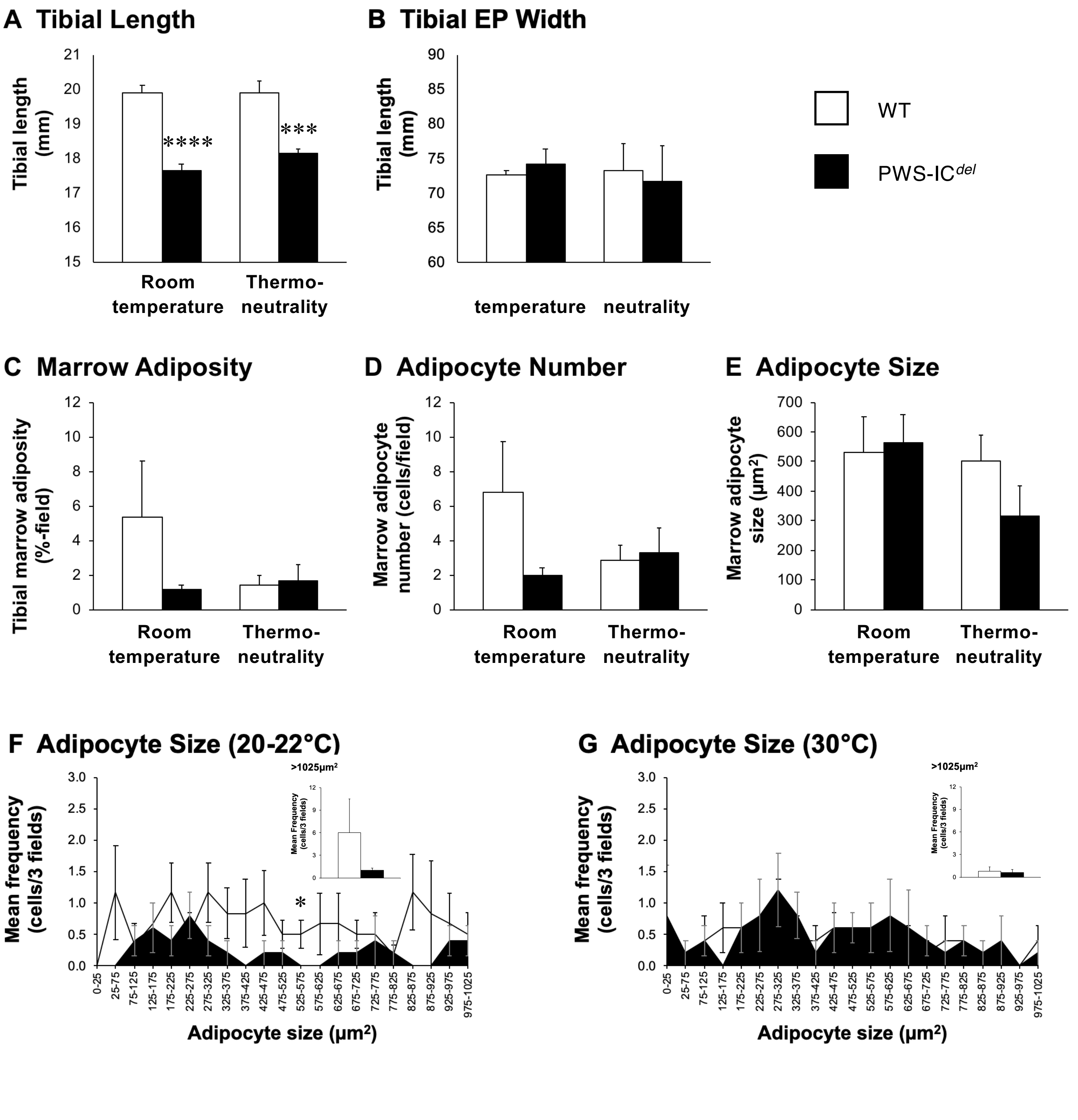

Figure 6: Thermoneutrality has little effect on growth and marrow adiposity in PWS-IC*del* mice. Tibial length (A), epiphyseal plate (EP) width (B), marrow adiposity (C), adipocyte number (D) and mean adipocyte size (E) were quantified in 6-15-month old male WT and PWS-IC*del* after being maintained at either standard ambient temperature (20-22˚C) or thermoneutrality (30˚C) for 9 weeks. Adipocyte size profiles are presented for standard ambient temperature (F) and thermoneutrality (G). Data shown are mean ± SEM (n=6 (room temperature) and 5 (thermoneutrality)), with statistical comparisons performed by 1-way ANOVA and Bonferroni post hoc test (A-E; **** P<0.0001 vs room temperature (same genotype)) or unpaired Student's t-test (F & G; * P<0.05 vs WT littermates (same temperature)).

Braxton TM *et al*, 2019; Figure 7

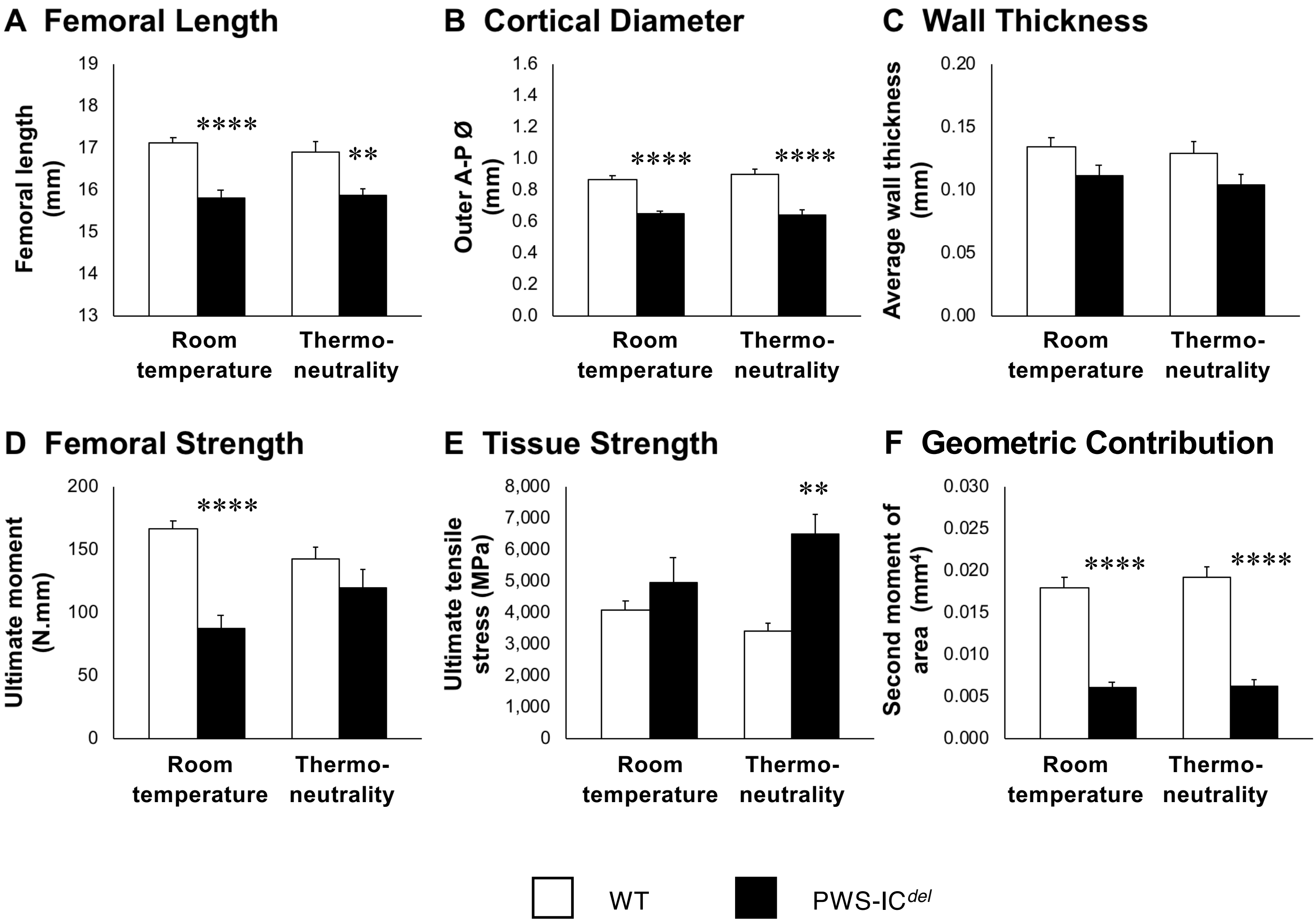

Figure 7: Thermoneutrality has little effect on growth and marrow adiposity in PWS-IC*del* mice. Tibial length (A), epiphyseal plate (EP) width (B), marrow adiposity (C), adipocyte number (D) and mean adipocyte size (E) were quantified in 6-15-month old male WT and PWS-IC*del* after being maintained at either standard ambient temperature (20-22˚C) or thermoneutrality (30˚C) for 9 weeks (n=6 (room temperature) and 5 (thermoneutrality)). Data shown are mean ± SEM, with statistical comparisons performed by 1-way ANOVA and Bonferroni post hoc test (***P*<0.01; *****P*<0.0001 vs WT littermates (same ambient temperature)).